Journal of Science, Innovation and Creativity
Vol. 5 No. 2 (2026): ISSN (Online): 2958-454X
DOI:
Buongiorno Model of Magnetohydrodynamic Nanofluid Flow Over a Heated Stretching Sheet

Buongiorno Model of Magnetohydrodynamic Nanofluid Flow Over a Heated Stretching Sheet

Mary Joan Oluoch & Winifred Mutuku
Kenyatta University, Kenya

Article History
Received: 2026-06-12
Revised: 2026-09-30
Accepted: 2026-10-11
Published: 2026-10-18

Keywords
Diffusion
Magnetohydrodynamic
Nanofluid
Thermophoresis

How to cite:
Oluoch, M. J., & Mutuku, W. (2026). Buongiorno Model of Magnetohydrodynamic Nanofluid Flow Over a Heated Stretching Sheet. *Journal Science, Innovation and Creativity, 5*(2), 258-273.

Copyright © 2026

Abstract
Nanofluids are important working fluids for electronic cooling in industrial, engineering, and biomedical applications. Although magnetohydrodynamic (MHD) nanofluid flow over stretching sheets has been widely studied, the combined effects of viscous dissipation, thermophoresis, Brownian motion, and a magnetic field under the Buongiorno model remain insufficiently explored. This study numerically investigates these effects, along with Joule heating and convective surface heating, on flow over a heated stretching sheet subject to a perpendicular magnetic field. Similarity transformations were used to reduce the governing partial differential equations of continuity, momentum, energy, and concentration to nonlinear first-order ordinary differential equations. The resulting boundary value problem was solved using the shooting technique with the Runge–Kutta method in the MATLAB ode45 function. Results show that the magnetic field increases the temperature through Joule heating and diminishes the convective flow through the Lorentz force. Brownian motion and thermophoretic parameters elevate the nanoparticle distribution and increase the fluid temperature. The Eckert number intensifies viscous heating, while the Prandtl number restricts thermal diffusion. The Schmidt number decreases species concentration, while the Joule heating parameter enhances the temperature near the surface. The skin friction increases with the magnetic parameter while the Sherwood number decreases; a higher Prandtl number enhances heat transfer but reduces mass transfer, and the Nusselt number increases with the Biot number. These findings indicate that magnetic field strength and convective surface heating can be regulated to control wall shear stress and heat and mass transfer rates in plastic extrusion, metallurgy, and electronic cooling.

Introduction

In recent years, the manufacturing and engineering industries have shown increased demand for techniques that enhance heat transfer. In response, Choi and Eastman (1995), by dispersing nanoparticles in base fluids, introduced an improved heat transfer fluid called nanofluids. Research has explored the use of nanofluids in fields such as food production, biomedicine, electronics, and transportation. The improved properties of nanofluids are important in both experimental and theoretical investigations. Researchers, such as Wong and De Leon (2010), explored the behavior of nanofluids across various industrial applications, including electronics, biomedicine, food production, and transportation.

The Buongiorno model has been used to investigate the effect of the rapid, erratic zigzag movement of particles and thermodiffusion on nanofluid flow under different geometries. This model was proposed by Buongiorno (2006), and it uses two transport mechanisms:

thermophoresis and Brownian motion, to explain energy transport and the concentration of nanoparticles in the fluid in laminar flow.

Raza et al. (2022) applied the Buongiorno model to investigate the effect of magnetic field strength on the Darcy-Forchheimer stagnation point over a porous rotating medium. They proposed that the existence of dual solutions for stagnation point flow is physically stable for only one solution. Khan et al. (2017) employed the two-phase model proposed by Buongiorno (2006) to study three-dimensional nanofluid flow over a rotating disk. The results showed that the temperature was only marginally affected by variations in the Brownian motion parameter, whereas it increased with the thermophoresis (Soret) parameter.

Mishra and Kumar (2021) applied the two-phase Buongiorno model to study nanofluid flow with viscous dissipation, heat generation, and absorption. The flow was considered past a wedged porous medium, and they inferred that the temperature rise resulted from increased viscous dissipation and heat absorption or generation parameters. Aladdin et al. (2020) used the two-phase model proposed by Buongiorno to examine the stability of a two-dimensional stagnation point flow of a hydromagnetic nanofluid. The results showed a linearly stable solution and a linearly unstable solution.

Ganga et al. *(*2016) investigated the effect of heat generation and absorption using the two-phase model proposed by Buongiorno to investigate a two-dimensional boundary layer nanofluid flow past a vertical plate. The study showed that the velocity of the fluid increased with an increase in heat absorption and decreased with heat generation. Mustafa (2017) employed the two-phase Buongiorno model to investigate the effect of partial slip on MHD nanofluid flow past a rotating surface. The results revealed that both magnetic fields and velocity slip reduce the velocity profiles and the boundary layer thickness.

Daniel et al. *(*2017) also employed the two-phase model used by Buongiorno to examine the combined effects of viscous dissipation, Joule heating, and thermal radiation on a 2-D MHD nanofluid flow past a porous linearly stretching sheet. They concluded that the increased thermal stratification decreased the rate of transfer of heat and mass of the particles. Rahman et al. *(*2014) employed the two-phase model to study heat transfer characteristics on a steady nanofluid flow over a permeable exponentially shrinking or stretching sheet. Their results showed that dual solutions existed for the stagnation point flow, with instability and stability cases realized in the lower and the upper branches, respectively. Ratha et al. (2023) analyzed the effect of a magnetic field on unsteady 2D Casson nanofluid using the Buongiorno model on a horizontally shrinking sheet. They found that both Casson suction and injection parameters enhanced the fluid temperature and velocity.

Roşca et al. (2023) used the Buongiorno model to determine the stability analysis of steady three-dimensional nanofluid stagnation point flow past a non-linear permeable plate. Their results indicated the existence of dual solutions at intervals of shrinking and velocity slip parameters, with a greater effect evident on the second-order slip as opposed to the first-order slip. Zaimi et al. (2014) investigated nanofluid flow over permeable shrinking or stretching surfaces using Buongiorno's model, incorporating passively controlled nanoparticle fraction and second-order slip. Their results agree with those of Roşca et al. (2023). Ibrahim et al. (2013) studied the effect of a magnetic field on a nanofluid stagnation point flow in the presence of heat and mass transfer. Their results showed that increasing the velocity at the free stream led to a significant increase in the rate of heat transfer at the surface. Haq et al. (2015) studied the effects of thermal slip and magnetic field on a stagnation point flow of a nanofluid past a stretching sheet. The results showed that an increase in the magnetic field and thermal slip parameters led to a decrease in the fluid velocity and temperature, respectively. Khashi'ie et al. *(*2022) conducted a stability analysis on stagnation-point flow of a hybrid nanofluid subjected to a magnetic field. They found that there were dual solution branches, with the first one being stable. They also found that increasing the

magnetic parameter increased the heat transfer processes. In related work, Mutuku-Njane and Makinde (2013) analyzed the effects of Navier slip and buoyancy forces on the boundary layer flow of hydromagnetic nanofluid past a vertically heated porous medium. Their study showed that an increase in the magnetic field strength led to an increase in both the fluid temperature and the boundary layer thickness. Ghosh and Mukhopadhyay (2018) analyzed heat and mass transfer in a steady boundary layer flow of nanofluid past a porous medium that is exponentially shrinking. Their findings indicated that the fluid temperature and nanoparticle volume fraction increased with an increase in the thermophoretic parameter. On the other hand, a decrease in the Lewis number led to an increase in heat transfer. Mutuku et al. (2014) investigated the MHD boundary layer flow of a nanofluid over a convectively heated flat plate, taking suction effects, magnetic field intensity, and viscous dissipation into consideration. They noted a retardation in the fluid field as the suction and magnetic field parameters increased. Significant changes in heat transfer rates and fluid temperature were also observed under the variation of various parameters. Jafar et al. (2012) studied the combined effects of Joule heating, external magnetic field, and viscous dissipation on a stagnation point nanofluid flow. They found distinct heat transfer characteristics between the shrinking and stretching sheets. In a different study, Pal and Mandal (2014) examined the effects of thermal radiation on mixed convection stagnation-point flow of nanofluids over a shrinking or stretching sheet in a porous medium with chemical reactions. They found that thermal radiation and chemical reactions enhance the rates of heat and mass transfer.

Similarly, Zhang et al. (2021) explored the effects of Joule heating and convection on two-dimensional MHD stagnation point flow on a curved shrinking or stretching surface. They found that a rise in magnetic field reduced the velocity profile due to the presence of the Lorentz force while simultaneously increasing the heat transfer and temperature profile due to Joule heating. Additionally, increasing the magnetic field also elevated both the Nusselt number and skin friction coefficients, indicating improved momentum and heat transfer.

Bachok et al. (2012) analyzed the two-dimensional stagnation-point flow of nanofluid over an exponentially shrinking or stretching sheet. Their study showed non-unique solutions for the shrinking sheets, with a dual solution emerging under certain scenarios. Consequently, nanoparticles enhanced the heat transfer rates and decreased boundary layer thickness. Sheikholeslami et al. (2014) conducted a numerical analysis of nanofluid flow and heat transfer between two horizontal parallel plates in the presence of viscous dissipation. Their findings demonstrated a direct relationship between the Reynolds number, Nusselt number, and nanoparticle volume fraction, and an inverse relationship with both the Eckert number and magnetic parameter. Additionally, an increase in the magnetic field parameter reduced the concentration profile while increasing skin friction.

Nadeem and Haq (2015) used the Buongiorno model to examine the three-dimensional flow of MHD nanofluids past a porous shrinking sheet under the influence of thermal radiation. Their study revealed that thermophoresis and Brownian motion reduced the nanoparticle volume fraction, and the temperature profiles decreased with an increase in Prandtl number. The intensity of Sherwood and local Nusselt numbers increased with a rise in thermal radiation and reduced with a rise in Lewis number parameters, respectively. Makinde et al. (2013) analyzed the convective heat transfer and buoyancy effect in MHD stagnation-point flow of nanofluids past a stretching sheet. They found that the magnetic field and buoyancy force enhance heat transfer while decelerating the velocity profiles.

Alaidrous and Eid (2020) used a two-phase model to study viscous dissipation, Joule heating, thermal radiation, and slip effects on a radiative three-dimensional nanofluid flow over a surface immersed in a porous medium. Their findings showed that nanoparticle concentration and velocity decreased with an increase in porous medium and thermal radiation parameters, while the temperature rose due to an increase in thermal conductivity. Yashkun et al. (2023) explored

the effects of thermal radiation, heat source, slip, and suction on MHD stagnation-point flow and heat transfer over a stretching sheet. They observed that the increase in suction and Prandtl number reduced the boundary layer velocity and temperature, while permeability and radiation parameters increased the boundary layer thickness.

Arshad et al. (2022) investigated MHD nanofluid flow across an exponentially stretching sheet, incorporating Brownian motion and thermophoresis using a 2-phase model. Their findings indicated that an increase in magnetic field intensity reduced fluid velocity while increasing the temperature, whereas the heat and mass buoyancy forces enhanced the velocity. They also found that Brownian motion lowered nanoparticle concentration, while thermophoresis raised it. Tshivhi and Makinde (2023) conducted a stability analysis on stagnation-point flow of nanofluids toward a shrinking sheet using Joule heating, viscous dissipation, Brownian motion, and thermophoresis parameters within the Buongiorno model. They found that Brownian motion and the Eckert number diminished the Sherwood number, thermophoresis and the Biot number improved the rates of heat transfer, and that an increase in the surface slip and magnetic field parameters reduced the lower branch's velocity boundary-layer thickness. However, their study focused on dual solutions and stability analysis over a slippery surface. In contrast, the present study considers a no-slip stretching surface rather than the shrinking slippery surface with zero nanoparticle flux considered by Tshivhi and Makinde (2023), and focuses on how viscous dissipation, Joule heating, Brownian motion, and thermophoresis interact with convective surface heating to govern the skin friction coefficient, Nusselt number, Sherwood number, temperature, velocity, and concentration.

From the reviewed literature, it is known that the magnetic field decreases the fluid velocity through the Lorentz force and raises the temperature through Joule heating, while Brownian motion, thermophoresis, and viscous dissipation increase the fluid temperature. However, most of these studies considered stretching sheets, stagnation-point flows, rotating disks, or porous media, and many focused on dual solutions and stability analysis. Additionally, how these heating mechanisms compete with one another and with convective heating at the surface to control the wall shear stress and the rates of heat and mass transfer has been underexplored.

Motivated by the reviewed literature, it is evident that the combined effect of viscous dissipation, thermophoresis, Brownian motion, and magnetic fields on nanofluid flow over a convectively heated stretching sheet, particularly using the Buongiorno model, has not been thoroughly investigated. Therefore, the objective of this study is to analyze MHD Buongiorno nanofluid flow over a heated stretching sheet with viscous dissipation, Joule heating, thermophoresis, Brownian motion, and convective heating at the surface, and to determine the effects of the pertinent parameters on the velocity, temperature, and concentration profiles as well as on the skin friction, Nusselt number, and Sherwood number. Unlike previous studies that focused mainly on dual solutions and stability, the contribution of this study is a parametric analysis that separates the thermal effects of viscous dissipation, Joule heating, and nanoparticle migration, explains the non-uniform effect of the Prandtl number on the temperature profile, and quantifies the resulting changes in the skin friction, Nusselt number, and Sherwood number.

Mathematical Formulation

This study considers a steady, two-dimensional, and incompressible flow. The fluid flows past a heated horizontal stretching sheet, where the x-axis is taken along the sheet, and the y-axis is normal to it, as shown in Figure 1. Magnetic field strength B_0 is imposed perpendicular to the motion of the nanofluid. It is assumed that the velocity of the stretching surface is $U_w = ax$, where a > 0 is the stretching rate, and the free stream velocity is U∞ = bx, the free stream temperature and concentration are T_w and C_w, while the ambient temperature and concentration are T_∞ and C_∞, respectively.

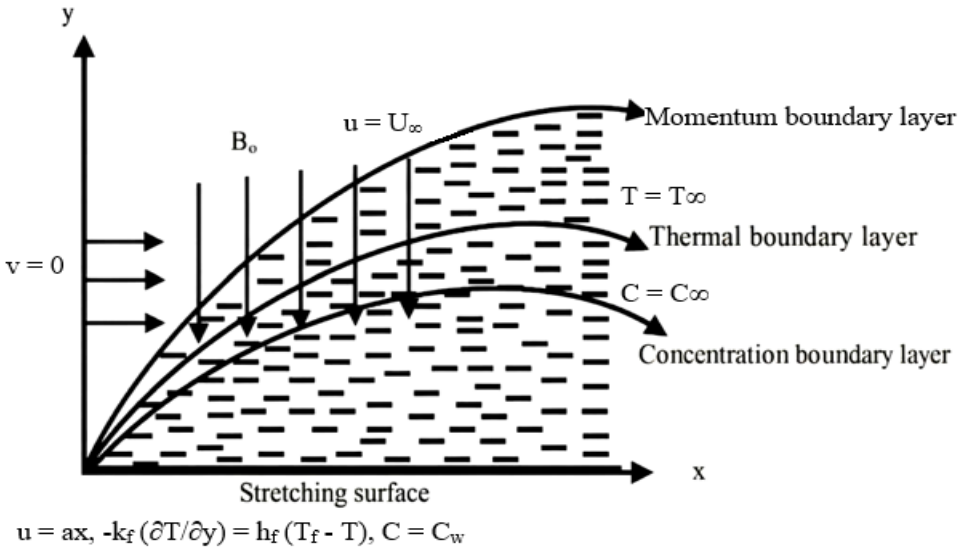


Figure 1: Geometry of the fluid flow

Based on the Buongiorno two-phase model, the boundary layer equations of continuity, momentum, energy, and concentration were formulated as follows.

$$\frac{\partial u}{\partial x}+\frac{\partial v}{\partial y}=0 \tag{1}$$

$$\mathrm{u}\frac{\partial u}{\partial x}+ v\frac{\partial u}{\partial y} = \frac{\mu}{\rho}\frac{\partial^2 u}{\partial y^2} - \frac{\sigma_{nf}}{\rho_{nf}}B_o^2(\mathrm{u}-U_\infty) \tag{2}$$

$$\mathrm{u}\frac{\partial T}{\partial x}+\mathrm{v}\frac{\partial T}{\partial y}=\alpha\frac{\partial^2 T}{\partial y^2}+ \frac{\mu}{\rho_{cp}}\left(\frac{\partial u}{\partial y}\right)^2 + \frac{\sigma}{\rho_{cp}}B_0^2(u- U_\infty)^2 + \tau\left[D_B\frac{\partial C}{\partial y}\frac{\partial T}{\partial y}+\frac{D_T}{T_\infty}\left(\frac{\partial T}{\partial y}\right)^2\right] \tag{3}$$

$$\mathrm{u}\frac{\partial C}{\partial x}+v\frac{\partial C}{\partial y}=D_B\frac{\partial^2 C}{\partial y^2}+\frac{D_T}{T_\infty}\frac{\partial^2 T}{\partial y^2} \tag{4}$$

With boundary conditions defined as:

$$\left.\begin{array}{l}\text{At y} = 0,\ \mathrm{u} = U_w(x) = ax,\ \mathrm{v} = 0,\ -k_f\frac{\partial T}{\partial y} = h_f(T_f - T), C = C_w \\ y \to \infty, \mathrm{T} \to T_\infty, \mathrm{C} \to C_\infty, \mathrm{u} = U_\infty(x) = bx\end{array}\right\} \tag{5}$$

The similarity transformation variables, free stream, and the equipotential functions are stated as follows to convert the partial differential equations 1-4 and the boundary condition 5 to a set of nonlinear ODEs.

$$\eta = y\left(\frac{a}{v}\right)^{\frac{1}{2}},\ \mathrm{T} = (T_f - T_\infty)\,\theta(\eta) + T_\infty, C = (C_{w-C_\infty})\,\phi(\eta) + C_\infty, u = \frac{\partial \psi}{\partial y},$$

$$v = -\frac{\partial \psi}{\partial x}, \Psi = x(av)^{\frac{1}{2}}f(\eta)$$

Substituting these variables into equations (1)–(5), the continuity equation (1) is satisfied, and equations (2)–(5) reduce to the following nonlinear ODEs, where primes denote differentiation with respect to η:

$$f''' + ff'' - (f')^2 - M(f' - \lambda) = 0 \tag{6}$$

$$\theta'' + P_r f\theta' + P_r E_c (f'')^2 + P_r E_c Q(f' - \lambda)^2 + N_b P_r \theta' \phi' + P_r N_t (\theta')^2 = 0 \quad (7)$$

$$\phi'' + S_c f\phi' + \frac{N_t \theta''}{N_b} = 0 \quad (8)$$

$$\left.\begin{array}{l} \text{At } \eta = 0,\ f' = 1, \theta' = -Bi\,(1 - \theta), f = 0, \phi = 1 \\ \eta \to \infty, f' = \lambda, \theta \to 0, \phi \to 0 \end{array}\right\} \quad (9)$$

Where $P_r, E_c, S_c, N_t, N_b, M, Q, \lambda$ represent the Prandtl number, Eckert number, Schmidt number, thermophoresis parameter, Brownian motion parameter, magnetic field parameter, Joule heating parameter, and velocity ratio parameter, respectively, and Bi $= \frac{h_f}{k_f}\left(\frac{\nu}{a}\right)^{\frac{1}{2}}$ is the Biot number.

$$P_r = \frac{\nu}{\alpha}, E_c = \frac{a^2 x^2}{C_p(T_f - T_\infty)}, N_t = \frac{\tau D_T (T_f - T_\infty)}{\nu T_\infty}, S_c = \frac{\nu}{D_B}, N_b = \frac{\tau D_B (C_w - C_\infty)}{\nu}, M = \frac{\sigma B_0^2}{\rho}, Q = \frac{\sigma B_0^2}{a\rho}, \lambda = \frac{b}{a}$$

Numerical Approach

The variables $g_1 = f, g_2 = f', g_3 = f'', g_4 = \theta, g_5 = \theta', g_6 = \phi$, and $g_7 = \phi'$ are introduced to reduce the ODEs (6–8) and the boundary conditions (9) to obtain the following system of first-order equations.

$$g_1' = g_2 \quad (10)$$

$$g_2' = g_3 \quad (11)$$

$$g_3' = -g_1 g_3 + (g_2)^2 + M(g_2 - \lambda) = 0, \quad (12)$$

$$g_4' = g_5 \quad (13)$$

$$g_5' = -\Pr g_1 g_5 - \Pr \mathrm{Ec}(g_3)^2 - \Pr \mathrm{Qec}(g_2 - \lambda)^2 - Nb g_5 g_7 - Nt(g_5)^2 \quad (14)$$

$$g_6' = g_7 \quad (15)$$

$$g_7' = -Sc\, g_1 g_7 - \frac{Nt}{Nb} g_5^1 \quad (16)$$

$$\left.\begin{array}{l} g_1 = 0, g_2 = 1, g_5 = -Bi, (1 - g_4), g_6 = 1 \\ g_2 = \lambda, g_4 \to 0, g_6 \to 0 \end{array}\right\} \quad (17)$$

The resulting system of first-order equations was solved using the shooting technique in conjunction with the Runge-Kutta based MATLAB solver ode45. The shooting method transforms the boundary value problem into an equivalent initial value problem by estimating the missing initial conditions. Appropriate initial guesses were supplied for the unknown boundary conditions and iteratively updated using a nonlinear root-finding function fsolve until the prescribed far-field boundary conditions were satisfied.

The numerical integration was carried out using a relative tolerance of 10^{-6} and an absolute tolerance of 10^{-8}. The iterative procedure was repeated until the far-field boundary conditions were satisfied within the specified convergence criteria. The adopted numerical settings provided stable solutions for the cases considered. The developed numerical scheme was subsequently employed to determine the velocity, temperature, and concentration profiles, together with the corresponding skin-friction coefficient, local Nusselt number, and local Sherwood number, for different values of the governing physical parameters.

To validate the accuracy of the numerical procedure, the present results were compared with those reported by Zaimi et al. (2014) for the local Nusselt number under the limiting case M=Ec=Nb=Nt=Q=0 and λ=1. The results presented in **Table 1** show very good agreement with the published data.

Table 1: Comparison of the present values of $-\theta'(0)$ with those of Zaimi et al. (2014) for various values of Pr when M=Ec=Nb=Nt=Q=0 and λ=1.

Pr	Zaimi et al. (2014)	Present Results
0.72	0.463145	0.475697
1.00	0.581977	0.592016
3.00	1.165246	1.170471
7.00	1.895403	1.899238
10.00	2.308004	2.311515

The physical quantities of interest are skin friction, Nusselt number, and Sherwood number, described as

$$C_f = \frac{\tau_w}{\rho_f U_w^2} = \frac{\mu\left(\frac{a}{\nu}\right)^{\frac{1}{2}} axf''}{\rho_f U_w^2} \tag{18}$$

$$N_u = \frac{xq_w}{k_f(T_f - T_\infty)} = \frac{hx}{K_f} = \frac{-K_f\left(\frac{a}{\nu}\right)^{\frac{1}{2}}\theta' x}{K_f} \tag{19}$$

$$S_h = \frac{xj_w}{D_B(C_w - C_\infty)} = \frac{x.j_w}{D_B} = \frac{-xD_B\left(\frac{a}{\nu}\right)^{\frac{1}{2}}\phi'}{D_B} \tag{20}$$

In dimensionless form, equations (18)–(20) are expressed as

$$\frac{C_f}{(R_{ex})^{\frac{1}{2}}} = f''(0), \frac{N_u}{\sqrt{R_{ex}}} = -\theta', \frac{S_h}{\sqrt{R_{ex}}} = -\phi' \tag{21}$$

Result and Discussion

This section presents a graphical analysis and examines the influence of pertinent parameters on velocity, temperature, and concentration profiles. Before the results are discussed, the reliability of the numerical scheme is confirmed by the limiting-case comparison with the results of Zaimi et al. (2014) described in the Numerical Approach section. It also highlights potential areas for further study.

Velocity Profile

Figure 2 shows that the velocity of the nanofluid reduces significantly near the stretching sheet as the magnetic field is varied from 0 to 1.6, resulting in a thinner boundary layer. The effect is attributed to the Lorentz force produced through the interaction between the electrically conducting fluid and the magnetic field. The force opposes the motion of the fluid, decreasing the transfer of momentum and causing a decline in velocity. Magnetic strength rises as the

opposing force intensifies. Joule heating further slows the fluid velocity decay near the stretching surface. The other parameters do not affect the velocity profile.

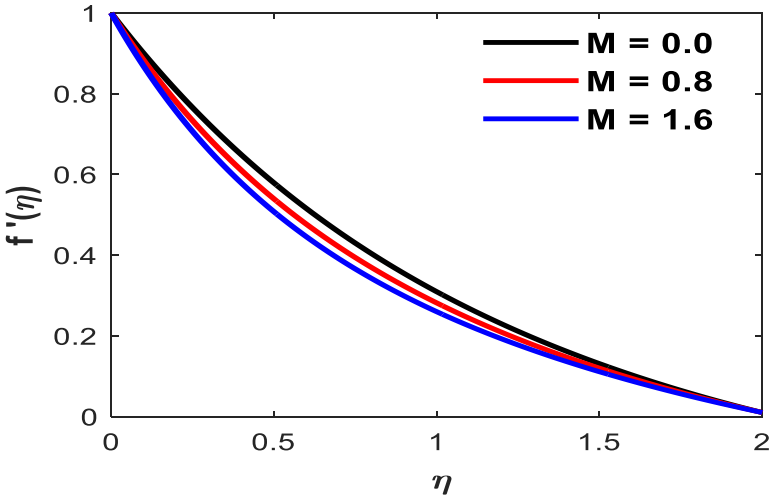


Figure 2: Effect of magnetic field on velocity

$\lambda = 0.01, \mathrm{Pr} = 2, \mathrm{Ec} = 0.5, \mathrm{Nb} = 0.2, \mathrm{Nt} = 0.3, \mathrm{Sc} = 0.6, \mathrm{Bi} = 0.1, \mathrm{Q} = 0.25$

Temperature Profile

Figure 3 depicts the temperature rise with the Brownian motion parameter, indicating an upward trend. This behaviour can be attributed to the Brownian motion term $N_b P_r \theta' \phi'$ appearing in the energy equation. This behavior is attributed to the increased Brownian motion of the nanoparticles, which intensifies nanoparticle diffusion and consequently strengthens the interaction between nanoparticle transport and heat transfer.

Figure 4 shows that an increase in the thermophoretic parameter boosts the temperature profile, particularly near the heated stretching sheet, and slowly levels off away from the boundary layer. As the thermophoretic parameter increases, nanoparticle transport induced by temperature gradients becomes more pronounced, enhancing thermal transport within the boundary layer. Consequently, the thermal boundary-layer thickness increases and higher temperatures are maintained throughout the fluid domain.

Figure 5 illustrates escalation of the magnetic parameter increases heat energy. This effect is caused by a strong temperature gradient, where the Lorentz force from the magnetic field retards the fluid motion, diminishing convective currents and leading to less heat dissipation. The thermal boundary layer thickens due to the accumulation of thermal energy near the stretching sheet. Additionally, Joule heating converts electrical energy to heat, consequently contributing to a rise in temperature.

Figure 6 shows that the effect of the Eckert number improves the heat energy of the fluid. The rising values indicate the availability of more kinetic energy relative to thermal capacity, which intensifies the viscous heating that results from the interaction between nanoparticles, particles of the base fluid, and kinetic energy and the velocity gradient. The magnetic braking further enhances the viscous heating, thus retaining the heat close to the surface.

Figure 7 shows that increasing the Prandtl number alters the temperature distribution and reduces the thermal boundary-layer thickness. Although the temperature near the wall increases slightly with Pr, the temperature decays more rapidly away from the surface, indicating reduced thermal diffusion and faster attainment of the ambient temperature.

Figure 8 shows that the temperature profile increases with increasing values of the Joule heating parameter Q. Higher values of Q enhance the amount of Joule heating generated within the electrically conducting fluid, resulting in an increase in fluid temperature and a thicker thermal boundary layer.

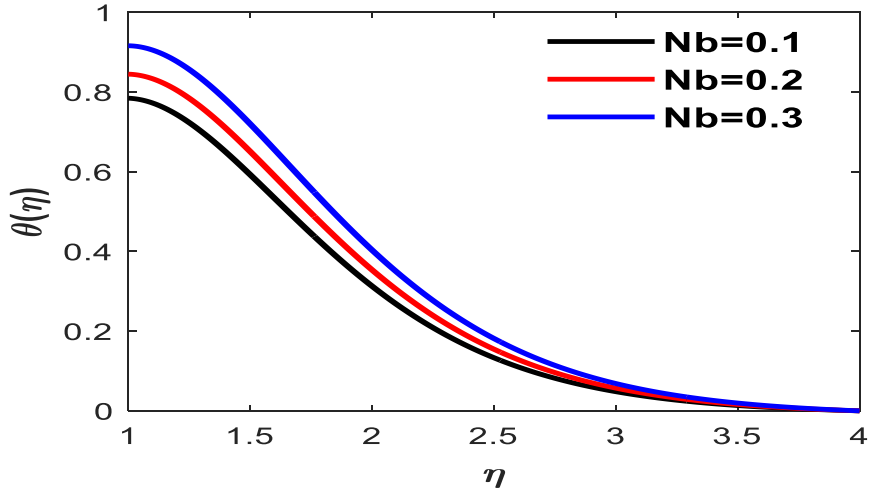


Figure 3: Effect of Brownian motion on temperature

$\lambda = 0.01, Ec = 0.5, Bi = 0.1, Q = 0.25, M = 0.25, Pr = 3, Sc = 0.4, Nt = 0.3$

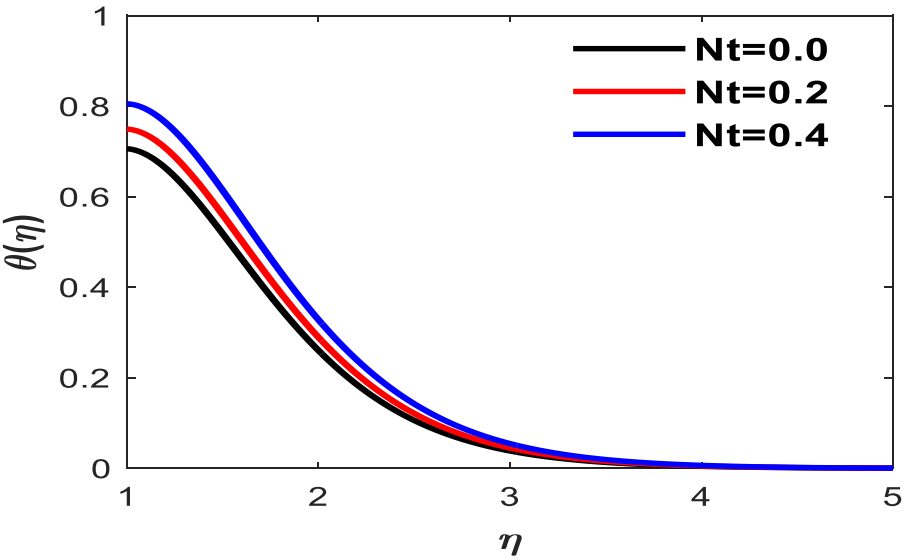


Figure 4: Effect of thermophoresis on temperature

$\lambda = 0.01, Ec = 0.5, Bi = 0.1, Q = 0.25, M = 0.25, Pr = 4, Sc = 0.4, Nb = 0.2$

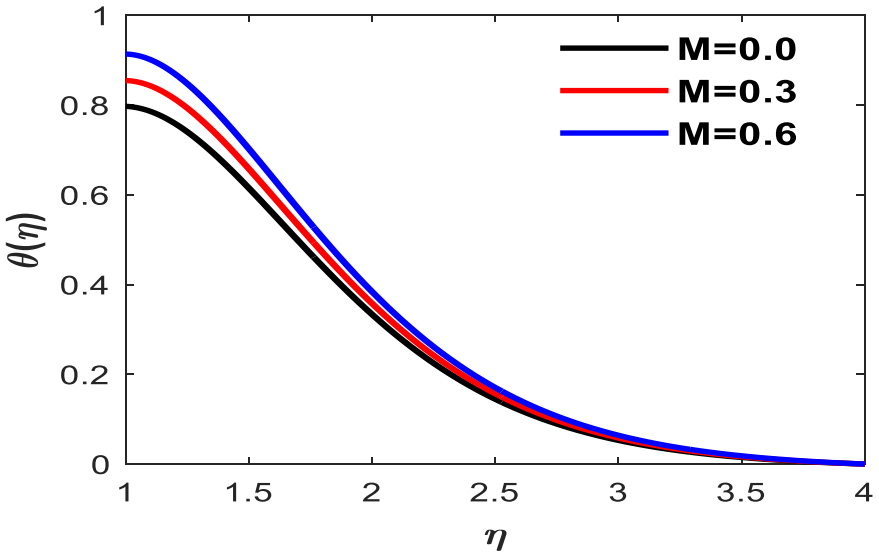


Figure 5: Effect of Magnetic field on temperature

$\lambda = 0.01, Ec = 0.5, Bi = 0.1, Q = 0.25, Nb = 0.2, Nt = 0.3, Pr = 4, Sc = 0.4$

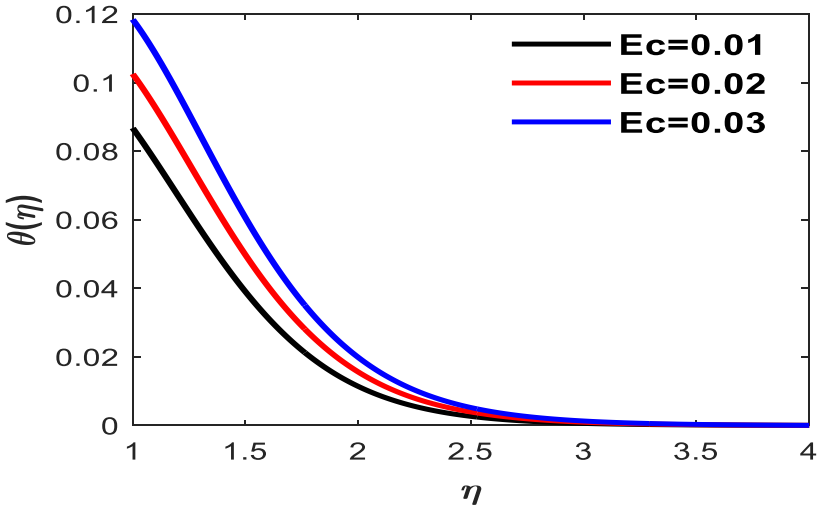


Figure 6: Effect of Eckert number on temperature

$\lambda = 0.01, Bi = 0.1, Q = 0.25, Nb = 0.2, Nt = 0.3, Pr = 5, Sc = 0.4, M = 0.25$

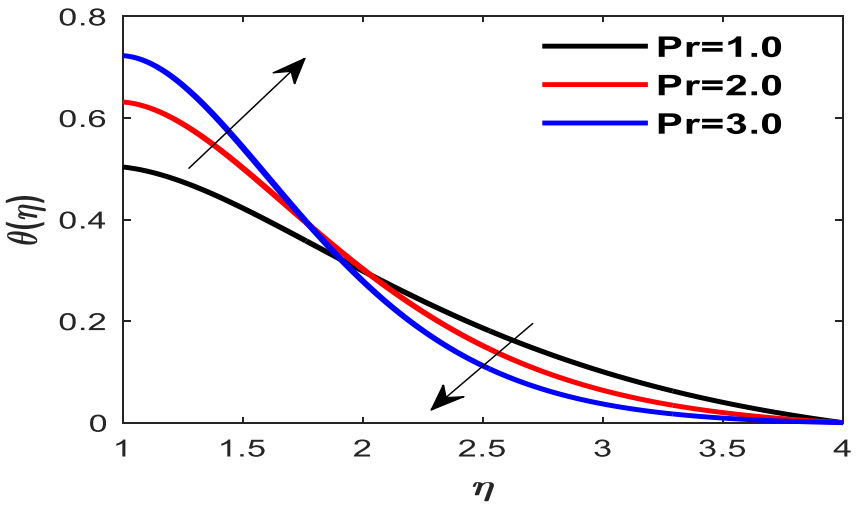


Figure 7: Effect of Prandtl number on temperature

$$\lambda = 0.01, Bi = 0.1, Q = 0.25, Nb = 0.2, Nt = 0.3, Sc = 0.4, M = 0.25, Ec = 0.5$$

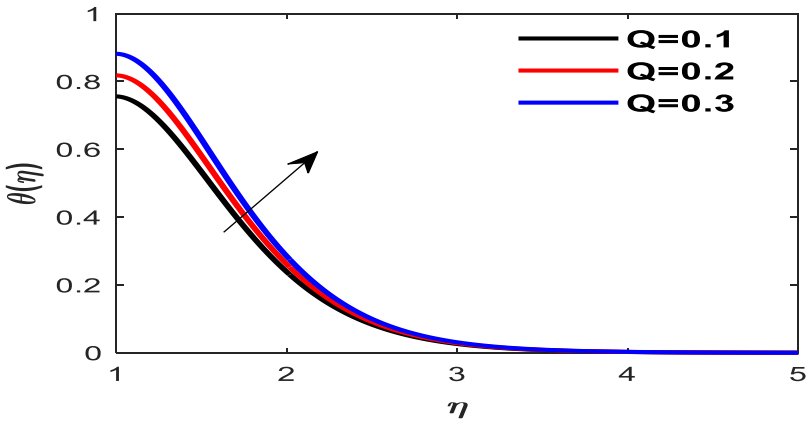


Figure 8: Effect of Joule heating parameter on temperature

$\lambda = 0.01, \mathrm{Bi} = 0.1, \mathrm{Nb} = 0.2, \mathrm{Nt} = 0.3, \mathrm{Sc} = 0.4, \mathrm{M} = 0.25, \mathrm{Ec} = 0.5, \mathrm{Pr} = 4$

Concentration Profile

Figure 9 shows that the concentration profile decreases with increasing Schmidt number. Since higher Schmidt numbers correspond to lower mass diffusivity, nanoparticle diffusion is reduced, leading to a thinner concentration boundary layer and lower concentration levels throughout the flow region.

Figure 10 illustrates the effect of the Joule heating parameter Q on the concentration profile. It is observed that increasing Q decreases the concentration distribution throughout the concentration boundary layer. Higher values of the Joule heating parameter increase the fluid temperature, which enhances thermal transport within the flow and alters nanoparticle distribution. Consequently, the concentration boundary-layer thickness decreases, resulting in lower concentration levels as Q increases.

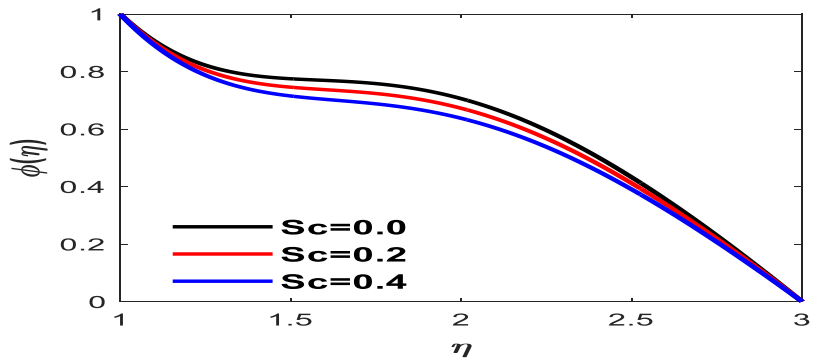


Figure 9: Effect of Schmidt number on concentration

$\lambda = 0.01, \mathrm{Bi} = 0.1, \mathrm{Nb} = 0.2, \mathrm{Ec} = 0.5, \mathrm{Q} = 0.25, \mathrm{Pr} = 5, \mathrm{M} = 0.25, \mathrm{Nt} = 0.2$

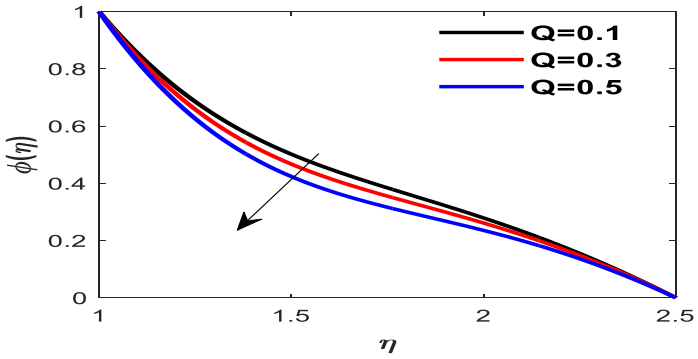


Figure 10: Effect of Joule heating parameter on concentration

$$\lambda = 0.01, Bi = 0.1, Nb = 0.2, Sc = 0.4, Ec = 0.5, Pr = 4, M = 0.25, Nt = 0.2$$

Table 2: Skin-Friction Coefficient, Local Nusselt Number, and Local Sherwood Number for Various Values of M, Pr, Bi, Sc, and Ec

Parameter	Value	$Cf_x Re_x^{\frac{1}{2}}$	$Nu_x Re_x^{-\frac{1}{2}}$	$Sh_x Re_x^{-\frac{1}{2}}$
M	0.1	-0.19719	0.28578	0.36444
	0.2	-0.19496	0.28754	0.36419
	0.3	-0.19279	0.28994	0.36348
	0.4	-0.19069	0.29295	0.36235
Pr	0.2	-0.18666	0.30074	0.35888
	0.4	-0.18666	0.39390	0.29080
	0.6	-0.18666	0.50993	0.20120
	0.8	-0.18666	0.66062	0.07792
Bi	0.5	–	0.37035	0.31465
	0.6	–	0.39087	0.30454
	0.7	–	0.40781	0.29609
	0.8	–	0.42203	0.28895
Sc	0.3	–	0.37178	0.38497
	0.6	–	0.37048	0.32105
	0.9	–	0.36917	0.25687
	1.2	–	0.36785	0.19241
Ec	0.1	–	0.29103	0.44758
	0.4	–	0.33946	0.42300
	0.7	–	0.38873	0.39770
	1.0	–	0.43883	0.37167

Columns 3–5 give f″(0), −θ′(0) and $-\phi'(0)$, respectively, as defined in equation (21). A dash (—) indicates that the skin-friction coefficient is unaffected, since Bi, Sc, and Ec do not appear in the momentum equation (6).

Table 2 presents the effects of the magnetic parameter M, Prandtl number Pr, Biot number Bi, Schmidt number Sc, and Eckert number Ec on the skin-friction coefficient $Cf_x Re_x^{\frac{1}{2}}$, local Nusselt number $Nu_x Re_x^{-\frac{1}{2}}$, and local Sherwood number $Sh_x Re_x^{-\frac{1}{2}}$.
Increasing the magnetic parameter M from 0.1 to 0.4 raises the skin-friction coefficient from −0.19719 to −0.19069 and the local Nusselt number from 0.28578 to 0.29295. Conversely, the local Sherwood number decreases slightly from 0.36444 to 0.36235. These results indicate that increasing magnetic field strength enhances heat transfer while reducing mass transfer.

The effect of the Prandtl number is shown by varying Pr from 0.2 to 0.8 while keeping the remaining parameters fixed. The skin-friction coefficient remains unchanged at −0.18666. However, the local Nusselt number increases considerably from 0.30074 to 0.66062, whereas the local Sherwood number decreases from 0.35888 to 0.07792. This behaviour indicates that increasing the Prandtl number enhances heat transfer at the surface while reducing mass transfer.

The influence of the Biot number is observed by increasing Bi from 0.5 to 0.8. The local Nusselt number increases, while the local Sherwood number decreases. Therefore, larger Biot numbers improve heat transfer from the surface but reduce mass transfer.

The effect of the Schmidt number is presented from 0.3 to 1.2. The local Nusselt number decreases slightly from 0.37178 to 0.36785, whereas the local Sherwood number decreases significantly from 0.38497 to 0.19241. These results show that increasing the Schmidt number suppresses mass transfer more strongly than heat transfer.

Finally, increasing the Eckert number from 0.1 to 1.0 results in an increase in the local Nusselt number, while the local Sherwood number decreases. Thus, higher values of the Eckert number enhance heat transfer but reduce mass transfer at the surface.

Conclusion
This study investigated the magnetohydrodynamic Buongiorno nanofluid flow over a heated stretching sheet in the presence of Brownian motion, thermophoresis, viscous dissipation, convective heating, and Joule heating effects. The governing partial differential equations were transformed into a system of nonlinear ordinary differential equations and solved numerically using a shooting technique coupled with the MATLAB ode45 solver. The effects of the governing parameters on the velocity, temperature, concentration, and transport characteristics were analyzed.

The major findings of the study are summarized as follows:

i. An increase in the magnetic parameter (M) reduces the velocity profile due to the resistive Lorentz force acting on the electrically conducting fluid. However, the temperature profile increases with increasing magnetic field strength owing to the enhanced Joule heating effect.

ii. Increasing the Brownian motion parameter (Nb) and thermophoretic parameter (Nt) elevates the temperature distribution within the boundary layer.

iii. The Eckert number (Ec) increases the fluid temperature due to viscous dissipation. In contrast, the Prandtl number (Pr) suppresses the temperature distribution and reduces the thermal boundary-layer thickness.

iv. The Joule heating parameter (Q) enhances the temperature profile throughout the boundary layer due to the additional thermal energy supplied to the fluid.

v. The Schmidt number (Sc) and the Joule heating parameter (Q) decrease the concentration profile.

vi. An important outcome of this study is that the governing parameters can be manipulated to regulate heat and mass transfer characteristics. In particular, increasing the magnetic parameter, Prandtl number, Biot number, and Eckert number enhances the rate of heat transfer, whereas increasing the Schmidt number suppresses mass transfer. This provides additional understanding of how transport processes can be controlled in magnetohydrodynamic Buongiorno nanofluid flow over heated stretching surfaces.

The present study extends existing investigations on Buongiorno nanofluid flow over stretching surfaces by simultaneously incorporating magnetic field effects, viscous dissipation, convective heating, Brownian motion, thermophoresis, and Joule heating. The results provide additional insight into the coupled heat and mass transfer mechanisms that arise in electrically conducting nanofluids and may be useful in the design of thermal systems involving stretching surfaces, electronic cooling devices, metallurgical processes, and related heat-transfer applications.

This study analyzed magnetohydrodynamic Buongiorno nanofluid flow over a heated stretching sheet. Future studies may extend the present work by considering hybrid nanofluids, unsteady three-dimensional flow, and the effects of porous media. The influence of additional physical effects such as thermal radiation, chemical reactions, and variable fluid properties may also be investigated to broaden the applicability of the model.

References

Aladdin, N. A. L., Bachok, N., & Anuar, N. S. (2020). MHD stagnation point flow in nanofluid over shrinking surface using Buongiorno's model: A stability analysis. *Journal of Advanced Research in Fluid Mechanics and Thermal Sciences, 76*(3), 12–24.

Alaidrous, A. A., & Eid, M. R. (2020). 3-D electromagnetic radiative non-Newtonian nanofluid flow with Joule heating and higher-order reactions in porous materials. *Scientific Reports, 10*(1), Article 14513. https://doi.org/10.1038/s41598-020-71543-4

Arshad, M., Hussain, A., Hassan, A., Haider, Q., Ibrahim, A. H., Alqurashi, M. S., Almaliki, A. H., & Abdussattar, A. (2022). Thermophoresis and Brownian effect for chemically reacting magneto-hydrodynamic nanofluid flow across an exponentially stretching sheet. Energies, 15(1), Article 143. https://doi.org/10.3390/en15010143

Bachok, N., Ishak, A., & Pop, I. (2012). Boundary layer stagnation-point flow and heat transfer over an exponentially stretching/shrinking sheet in a nanofluid. *International Journal of Heat and Mass Transfer*, *55*(25–26), 8122–8128.

Buongiorno, J. (2006). Convective transport in nanofluids. *Journal of Heat Transfer, 128*(3), 240–250. https://doi.org/10.1115/1.2150834

Choi, S. U. S., & Eastman, J. A. (1995). Enhancing thermal conductivity of fluids with nanoparticles. In D. A. Siginer & H. P. Wang (Eds.), *Developments and applications of non-Newtonian flows* (FED-Vol. 231/MD-Vol. 66, pp. 99–105). American Society of Mechanical Engineers. https://doi.org/10.1115/IMECE1995-0926

Daniel, Y. S., Aziz, Z. A., Ismail, Z., & Salah, F. (2017). Effects of thermal radiation, viscous and Joule heating on electrical MHD nanofluid with double stratification. *Chinese Journal of Physics, 55*(3), 630–651. http://dx.doi.org/10.1016/j.cjph.2017.04.001

Ganga, B., Ansari, S. M. Y., Ganesh, N. V., & Hakeem, A. A. (2016). MHD flow of Boungiorno model nanofluid over a vertical plate with internal heat generation/absorption. *Propulsion and Power Research*, *5*(3), 211–222. http://dx.doi.org/10.1016/j.jppr.2016.07.003

Ghosh, S., & Mukhopadhyay, S. (2018). Flow and heat transfer of nanofluid over an exponentially shrinking porous sheet with heat and mass fluxes. *Propulsion and Power Research, 7*(3), 268–275. http://dx.doi.org/10.1016/j.jppr.2018.07.004

Haq, R. U., Nadeem, S., Khan, Z. H., & Akbar, N. S. (2015). Thermal radiation and slip effects on MHD stagnation point flow of nanofluid over a stretching sheet. *Physica E: Low-Dimensional Systems and Nanostructures*, *65*, 17–23. http://dx.doi.org/10.1016/j.physe.2014.07.013

Ibrahim, W., Shankar, B., & Nandeppanavar, M. M. (2013). MHD stagnation point flow and heat transfer due to nanofluid towards a stretching sheet. *International Journal of Heat and Mass Transfer, 56*(1–2), 1–9. http://dx.doi.org/10.1016/j.ijheatmasstransfer.2012.08.034

Jafar, K., Nazar, R., Ishak, A., & Pop, I. (2012). MHD flow and heat transfer over stretching/shrinking sheets with external magnetic field, viscous dissipation and Joule effects. *The Canadian Journal of Chemical Engineering, 90*(5), 1336–1346.

Khan, J. A., Mustafa, M., Hayat, T., Turkyilmazoglu, M., & Alsaedi, A. (2017). Numerical study of nanofluid flow and heat transfer over a rotating disk using Buongiorno's model. *International Journal of Numerical Methods for Heat & Fluid Flow*, *27*(1), 221–234. https://doi.org/10.1108/HFF-08-2015-0328

Khashi'ie, N. S., Wahid, N. S., Md Arifin, N., & Pop, I. (2022). MHD stagnation-point flow of hybrid nanofluid with convective heated shrinking disk, viscous dissipation and Joule heating effects. *Neural Computing and Applications*, *34*(20), 17601–17613.

Makinde, O. D., Khan, W. A., & Khan, Z. H. (2013). Buoyancy effects on MHD stagnation point flow and heat transfer of a nanofluid past a convectively heated stretching/shrinking sheet. *International Journal of Heat and Mass Transfer, 62*, 526–533.

Mishra, A., & Kumar, M. (2021). Numerical analysis of MHD nanofluid flow over a wedge, including effects of viscous dissipation and heat generation/absorption, using Buongiorno model. *Heat Transfer, 50*(8), 8453–8474. https://doi.org/10.1002/htj.22284

Mustafa, M. (2017). MHD nanofluid flow over a rotating disk with partial slip effects: Buongiorno model. *International Journal of Heat and Mass Transfer, 108*, 1910–1916. http://dx.doi.org/10.1016/j.ijheatmasstransfer.2017.01.064

Mutuku, W. N., Kithome, S. M., & Awuor, K. O. (2014). Analysis of MHD thermal boundary layer flow of nanofluids over a convectively heated moving flat plate. *Journal of Fluids and Thermal Sciences, 2*(1), 1.

Mutuku-Njane, W. N., & Makinde, O. D. (2013). Combined effect of buoyancy force and Navier slip on MHD flow of a nanofluid over a convectively heated vertical porous plate. *The Scientific World Journal, 2013,* Article 725643. https://doi.org/10.1155/2013/725643

Nadeem, S., & Haq, R. U. (2015). MHD boundary layer flow of a nanofluid passed through a porous shrinking sheet with thermal radiation. *Journal of Aerospace Engineering*, 28(2), Article 04014061. http://dx.doi.org/10.1061/(ASCE)AS.1943-5525.0000299

Pal, D., & Mandal, G. (2014). Influence of thermal radiation on mixed convection heat and mass transfer stagnation-point flow in nanofluids over stretching/shrinking sheet in a porous medium with chemical reaction. *Nuclear Engineering and Design, 273*, 644–652. http://dx.doi.org/10.1016/j.nucengdes.2014.01.032

Rahman, M. M., Roşca, A. V., & Pop, I. (2014). Boundary layer flow of a nanofluid past a permeable exponentially shrinking/stretching surface with second order slip using Buongiorno's model. *International Journal of Heat and Mass Transfer, 77*, 1133–1143.

Ratha, P. K., Mishra, S., Tripathy, R., & Pattnaik, P. K. (2023). Analytical approach on the free convection of Buongiorno model nanofluid over a shrinking surface. *Proceedings of the Institution of Mechanical Engineers, Part N: Journal of Nanomaterials, Nanoengineering and Nanosystems, 237*(3–4), 83–95. https://doi.org/10.1177/2397791422110

Raza, J., Dero, S., Lund, L. A., & Omar, Z. (2022). Duality and stability of MHD Darcy–Forchheimer porous medium flow of rotating nanofluid on a linear shrinking/stretching sheet: Buongiorno model. *International Journal of Numerical Methods for Heat & Fluid Flow, 32*(5),

1517–1539. https://doi.org/10.1108/HFF-01-2021-0054

Roşca, N. C., Roşca, A. V., & Pop, I. (2023). Dual solutions on three-dimensional nanofluid flow and heat transfer over a permeable non-linearly shrinking surface with second-order velocity slips. *International Journal of Numerical Methods for Heat & Fluid Flow*, *33*(7), 2392–2408. https://doi.org/10.1108/HFF-10-2022-0624

Sheikholeslami, M., Abelman, S., & Ganji, D. D. (2014). Numerical simulation of MHD nanofluid flow and heat transfer considering viscous dissipation. *International Journal of Heat and Mass Transfer*, *79*, 212–222. http://dx.doi.org/10.1016/j.ijheatmasstransfer.2014.08.004

Tshivhi, K. S., & Makinde, O. D. (2023). Dual solutions and stability analysis for Buongiorno model of magnetohydrodynamics nanofluid flow past a heated shrinking slippery surface. *Journal of Nanofluids, 12*(6), 1485–1494. https://doi.org/10.1166/jon.2023.2032

Wong, K. V., & De Leon, O. (2010). Applications of nanofluids: Current and future. *Advances in Mechanical Engineering, 2*, Article 519659. https://doi.org/10.1155/2010/51965

Yashkun, U., Zaimi, K., & Lund, L. A. (2023). MHD stagnation point flow with thermal radiation and slip effect over a linear stretching sheet. *Journal of Mountain Area Research*, *8*, 49–59. https://doi.org/10.53874/jmar.v8i0.175

Zaimi, K., Ishak, A., & Pop, I. (2014). Flow past a permeable stretching/shrinking sheet in a nanofluid using two-phase model. *PLOS ONE, 9*(11), Article e111743. https://doi.org/10.1371/journal.pone.0111743

Zhang, X. H., Abidi, A., Ahmed, A. E. S., Khan, M. R., El-Shorbagy, M. A., Shutaywi, M., Issakhov, A., & Galal, A. M. (2021). MHD stagnation point flow of nanofluid over a curved stretching/shrinking surface subject to the influence of Joule heating and convective condition. Case Studies in Thermal Engineering, 26, Article 101184. https://doi.org/10.1016/j.csite.2021.101184